Heliyon 9 (2023) e18132

Contents lists available at ScienceDirect

Heliyon

journal homepage: www.cell.com/heliyon

Identification of the relationship between single-cell N6-methyladenosine regulators and the infiltrating immune cells in esophageal carcinoma

Yunyi Bian [1], Guoshu Bi [1], Guangyao Shan [1], Jiaqi Liang, Guangyu Yao, Qihai Sui, Zhengyang Hu, Cheng Zhan, Zhencong Chen [**], Qun Wang [*]

Department of Thoracic Surgery, Zhongshan Hospital, Fudan University, Shanghai, China

ARTICLE INFO

Keywords:
Esophageal squamous carcinoma
N6-methyladenosine
Tumor microenvironment
Single-cell
Cell communication

ABSTRACT

Background: N6-methyladenosine (m^6A) RNA methylation plays a crucial role in important genomic processes in a variety of malignancies. However, the characterization of m^6A with infiltrating immune cells in the tumor microenvironment (TME) in esophageal squamous carcinoma (ESCC) remains unknown.

Methods: The single-cell transcriptome data from five ESCC patients in our hospital were analyzed, and TME clusters associated with prognosis and immune checkpoint genes were investigated. Cell isolation and qPCR were conducted to validate the gene characterization in different cells.

Results: According to distinct biological processes and marker genes, macrophages, T cells, and B cells clustered into three to four different subgroups. In addition, we demonstrated that m^6A RNA methylation regulators were strongly related to the clinical and biological features of ESCC. Analysis of transcriptome data revealed that m^6A-mediated TME cell subsets had high predictive value and showed a close relationship with immune checkpoint genes. The validation results from qPCR demonstrated the characteristics of essential genes. CellChat analysis revealed that RNA from TME cells m^6A methylation-associated cell subtypes had substantial and diversified interactions with cancer cells. Further investigation revealed that MIF- (CD74+CXCR4) and MIF-($CD74^+$CD44) ligand-receptor pairings facilitated communication between m^6A-associated subtypes of TME cells and cancer cells.

Conclusion: Overall, our study demonstrated for the first time the function of m^6A methylation-mediated intercellular communication in the microenvironment of tumors in controlling tumor development and anti-tumor immune regulation in ESCC.

1. Introduction

Esophageal cancer (EC), the sixth greatest cause of cancer deaths worldwide (5.3% of all cancer deaths), accounted for an estimated

* Corresponding author.
** Corresponding author.
E-mail addresses: zcchen13@fudan.edu.cn (Z. Chen), wang.qun@zs-hospital.sh.cn (Q. Wang).
[1] Bian Yunyi, Guoshu Bi, and Guangyao Shan contributed equally to this work.

https://doi.org/10.1016/j.heliyon.2023.e18132
Received 29 January 2023; Received in revised form 6 July 2023; Accepted 7 July 2023
Available online 13 July 2023

508 585 cancer deaths in 2018 [1]. Esophageal squamous carcinoma (ESCC) and esophageal adenocarcinoma (EADC) differ in geographic patterns and etiologies, with ESCC accounting for nearly 90% of EC [2]. The prognosis for ESCC was poor, and the few treatment choices for ESCC were associated with the risk of recurrence following surgical removal [3]. Recent advances in immune therapy, such as checkpoint inhibitors pembrolizumab and nivolumab, outperformed chemotherapy in treating recurrent or metastatic ESCC [4]. Among predictors of immune checkpoint inhibitor (ICI) response, programmed cell death-ligand 1(PD-L1) [5] and tumor microenvironment (TME) are extremely promising [6,7]. A broader understanding of the molecular processes underlying ESCC may facilitate the development of novel techniques for the prevention and treatment of ESCC.

The modifications of post-transcriptional changes played a critical role in regulating the development and progression of ESCC [8,9], such as N6-methyladenosine (m^6A), which was the most prevalent internal changes in transcripts, including more than 50% eukaryotic methylation, have been recognized as major epigenetic regulators of mRNA stability, splicing, and translation [10], as well as the production of small, noncoding RNA [11]. Three sorts of m6A regulators exist: writers, erasers, and readers. The methyltransferase complex (MTC), often known as "writers," catalyzes m^6A. Demethylase, often known as an "eraser," eliminates m^6A. The RNA reader protein identifies m^6A, binds the RNA, and carries out the associated tasks [12]. Significantly, m^6A mRNA regulation is involved in carcinogenesis, tumor formation, and metastasis. A previous study found that METTL3, the catalytic subunit of the N6-adenosine-methyltransferase complex, increased ESCC metastasis via activating EGR1/Snail signaling in an m6A-dependent way, which reflected the role of m^6A in ESCC [13,14].

The tumor microenvironment (TME), which consists of several stromal and tumor cells, was demonstrated to be associated with tumor progressions such as proliferation, invasion, metastasis, and treatment resistance [15,16]. Moreover, single-cell transcriptomics reveals distinct subtypes. TME cells and tumor cells communicate complexly [17–19]. TME cells consist of various cell types besides tumor cells, including tumor-associated macrophages (TAMs) [20,21], T cells, and B cells. Numerous studies have previously discovered that m^6A modifications have a significant role in the evolution of TME variety and complexity [22,23]. However, m^6A modification and subtypes of TME in ESCC need more investigation.

Here, we evaluated single cells from five ESCC tumor samples [24]. Sequencing data investigating the impact of m^6A mRNA methylation on major TME cells, including macrophages, T cells, and B cells, were analyzed. By 23 m^6A Non-negative matrix decomposition (NMF) clusters of RNA methylation regulators, as demonstrated previously [25], m^6A mRNA methylation differences were found in each ERCC TME cell type subgroup. The pattern demonstrated extensive and varied interactions with tumor epithelial cells and distinct immunity correlation between characteristics, transcriptional traits, and prognosis. Our study is the first to demonstrate that m^6A mRNA may drive intercellular communication between TME cells and tumor cells, hence accelerating the progression of ESCC.

2. Materials and methods

2.1. Ethics statement

The study was approved by the Ethics Committee of Zhongshan Hospital, Fudan University (B2021 137R).

2.2. Data preprocessing

We obtained the scRNA-seq and clinical data from patients diagnosed with ESCC and who received surgical treatment in the Department of Thoracic Surgery at Zhongshan Hospital, Fudan University (five ESCC and five corresponding noncancerous samples) (FDZSH). Several centimeters away from the tumor, noncancerous tissue samples were obtained from matched individuals and examined histopathologically to confirm the absence of tumor cells. Other ten ESCC and ten normal samples were chosen for qRT-PCR analysis. ESCC RNA-seq data were obtained from the UCSC Xena Browser and the GEO database (GSE53625) [26]. The preparation of the single-cell suspensions, single-cell RNA-seq data preprocessing, and analysis of 10x scRNA-seq data can be found in previous research [24,27]. The scRNA-seq data analysis was performed using R with cell filtering. The R package DoubletFinder was used to detect doublets [28]. The R package batchelor was used to remove batch effects [29]. The Seurat R package was used to analyze scRNA-seq data, including detecting highly variable genes, principal component analysis (PCA) dimension reduction, t-distributed stochastic neighbor embedding (TSNE) analysis, cell clustering analysis and detecting gene expression markers. Finally, based on the SingleR package, CellMarker dataset and previous reports, we annotated different cell types.

2.3. Non-negative matrix factorization of m^6A mRNA regulators TME cells

We used the NMF R package [30] to analyze the 23 m^6A regulators in all TME cell types and identified different cell subtypes for these cell types depending on the scRNA expression matrix to observe best the effect of m^6A-mediated regulator expression on TME cell types.

2.4. Analysis of marker genes for subtypes of m^6A-related cells in TME cells

Using the Findallmarkers function, we compiled a list of the markers of each NMF cluster in each ERCC cell type. The threshold was set as adjusted p-value <0.01 and fold change>0.5. We displayed the dominant expressed genes in each NMF cluster. The high-risk genes for ESCC reported in previous research were mentioned [31].

2.5. Functional enrichment analysis

To show the significance of the pathways involved, subclusters of marker genes in different TME cells were subjected to gene ontology (GO) and Kyoto Encyclopedia of Genes and Genomes (KEGG) enrichment analysis using the R package cluster profile. Adjusted p-value < 0.05 and false discovery rate (FDR) < 0.05 established the GO and KEGG analysis threshold.

2.6. Analysis of cell-to-cell communication

We used a previously reported R package, CellChat [32] and CellChatDB, to display the network between the cell-to-cell communication, which comprises ligand-receptor interaction databases that can evaluate intercellular communication networks using scRNA-seq data labeled with distinct cell clusters. The communication networks were shown as follows: (1) CellChat was used to illustrate the important cellular pathways involved in cell clustering. (2) netVisual circle is utilized to depict the network of cell clusters relative to other cell clusters in NMF. (3) The netVisual_bubble was used to display the interactions of ligand-receptor crosstalk among cell clusters.

2.7. Survival analysis

We applied CIBERSORTx [33] and the single-sample gene set enrichment analysis [34] (ssGSEA) tool to analyze the survival characterization in bulk RNA-sequence datasets. Based on the m^6A-related gene signature matrix we constructed before, we put the expression profiles in the scRNA data. The ssGSEA tool was used to compute these gene signature scores. Based on the median value of ssGSEA m^6A-related NMF signatures' score, we divided patients in the TCGA database into two groups: high and low expression. We illustrated the overall survival (OS) and recurrence-free survival (RFS) difference using a Kaplan-Meier survival curve generated by the ggplot2 software and set the p-value < 0.05 to show a statistically significant difference. To highlight the significance of differences in prognosis, the Log-rank test and COX analysis were utilized.

2.8. Analysis of immunotherapy transcriptome data

We downloaded the FPKM transcriptome data in 12 cohorts that received immune checkpoint blockade therapy from the public database as follows: MAGE A3 [35], PD1 blockade [36–41], CTLA4 [42], and PD1 blockade + CTLA4 [43,44], adoptive T cell therapy [45], and immune checkpoint inhibition [46]. All patients in these cohorts had the immunological response.

2.9. Statistical examination

R studio (4.1) was adopted to conduct all the statistical analysis. The significance of statistics was set as p-value$<$0.05. We used the Wilcoxon test, Kruskal–Wallis test, and Chi-square test for comparing continuous target or category variables in these subgroups of cells. Using Pearson analysis, the association between distinct cell signatures or gene expressions among TME ERCC cell types was determined.

2.10. Single-cell suspension processing

All samples were treated in the following method: Each sample was disrupted and digested in a MACS C Tube containing 200 mL of enzyme H, 25 mL of enzyme A, 100 mL of enzyme R, and 4.7 mL of Dulbecco's Modified Essential Medium for 30 min at 37 °C. Single-cell suspension was filtered using a 40-μm nylon mesh to eliminate cell aggregates and any remaining big particles. Red Blood Cell Lysis Solution (10 pounds) (Sigma-Aldrich, St. Louis, Missouri, United States) and Dead Cell Removal Kit (Miltenyi Biotec) were then used to extract erythrocytes and dead cells, respectively. $CD14^+$ macrophages were sorted using anti-CD14 magnetic beads. Pan T cells and B cells were obtained via related MACS magnetic microbeads (Miltenyi Biotec) according to the manufacturer's instructions.

2.11. RNA extraction and quantitative real-time polymerase chain reaction

TRIzol (Tiangen Biotechnology Co., Beijing, China) was used as an RNA extraction reagent. The cDNA template was produced using a PrimeScript RT Reagent Kit (TaKaRa, Tokyo, Japan), and quantitative real-time polymerase chain reaction was performed according to the manufacturer's instructions using SYBR Premix Ex Taq (TaKaRa). Each response was evaluated with the aid of QuantStudio 5 (Thermo Fisher Scientific). The 2-CT technique using GAPDH as the endogenous calibrator was used to objectively measure mRNA. Sangon Biotech provided the sequences for all primers.

3. Results

3.1. The characterization of m^6A associated with infiltrating immune cells in ESCC

The design of this study can be observed in Fig. 1A. We used a single-cell transcriptome dataset of ESCC from our hospital, as described previously, to study the characterization of m^6A RNA methylation regulators with infiltrating immune cells (Table S1). This

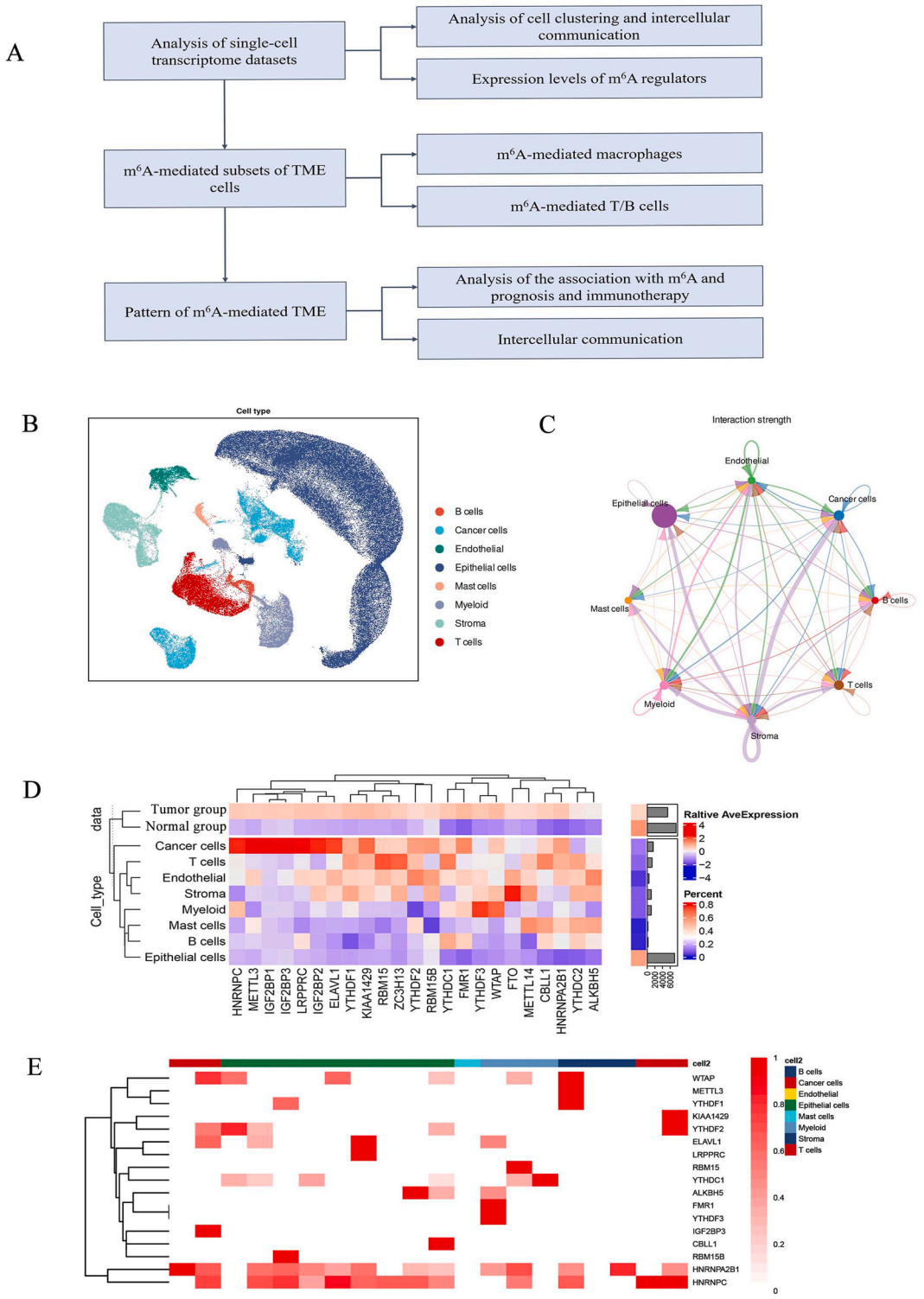

Fig. 1. Landscape single-cell data analysis of m^{6}A RNA regulators in ESCC. A: The flowchart showed the design of the study; **B**: Seurat t-distributed stochastic neighbor embedding (t-SNE) plot showed the cell distribution type; **C**: The network showed cell and cell interaction among the eight-cell types by Cellchat analysis; **D**: The heatmap displayed the expression level of the m^{6}A RNA regulators in tumor and normal groups from ESCC patients. **E**: The heatmap showed the distribution of m^{6}A RNA regulators in all eight-cell types.

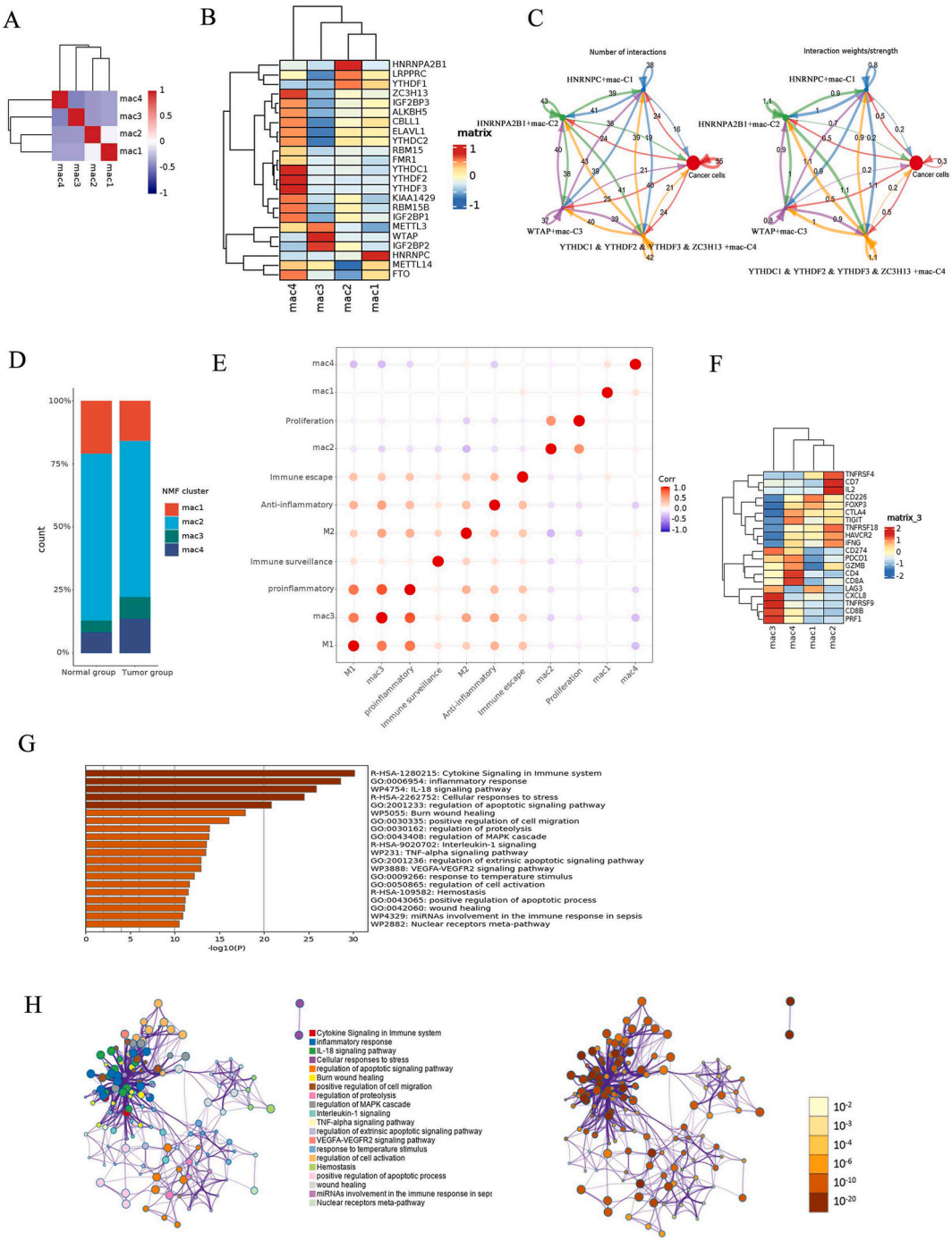

Fig. 2. The view of the interaction between the four different m^{6}A-associated macrophages clusters. A: The heatmap showed the correlation of the four m^{6}A-associated macrophages by NMF; **B**: The heatmap displayed the interactions between the m^{6}A-associated macrophages clusters and the cancer cells; **C**: Cell-to-cell interaction network between the m^{6}A-associated macrophages and cancer cells; **D**: The bar-plot revealed the different proportion of m^{6}A-associated macrophages clusters in the tumor and normal groups. **E** : The correlation plot showed the relationship between the different gene signatures with the m^{6}A-associated macrophage clusters; **F**: The heatmap revelated the relationship between the m^{6}A-associated macrophage clusters and the immune checkpoint-associated genes; **G**: G.O. and KEGG functional enrichment analysis of the genes in m^{6}A-associated macrophage clusters; **H**: Interactions between the enriched pathways across the genes in m^{6}A-associated macrophage clusters. The size of the dots denotes the number of genes in the relevant pathway, and the color indicates the cluster type. The paths for the clustering category are given in the tab on the label. Dots representing the same enrichment route have varied colors based on the p-value given on labels. The deeper the dots, the lower the p-value, and the more statistically significant it is. (For interpretation of the references to color in this figure legend, the reader is referred to the Web version of this article.)

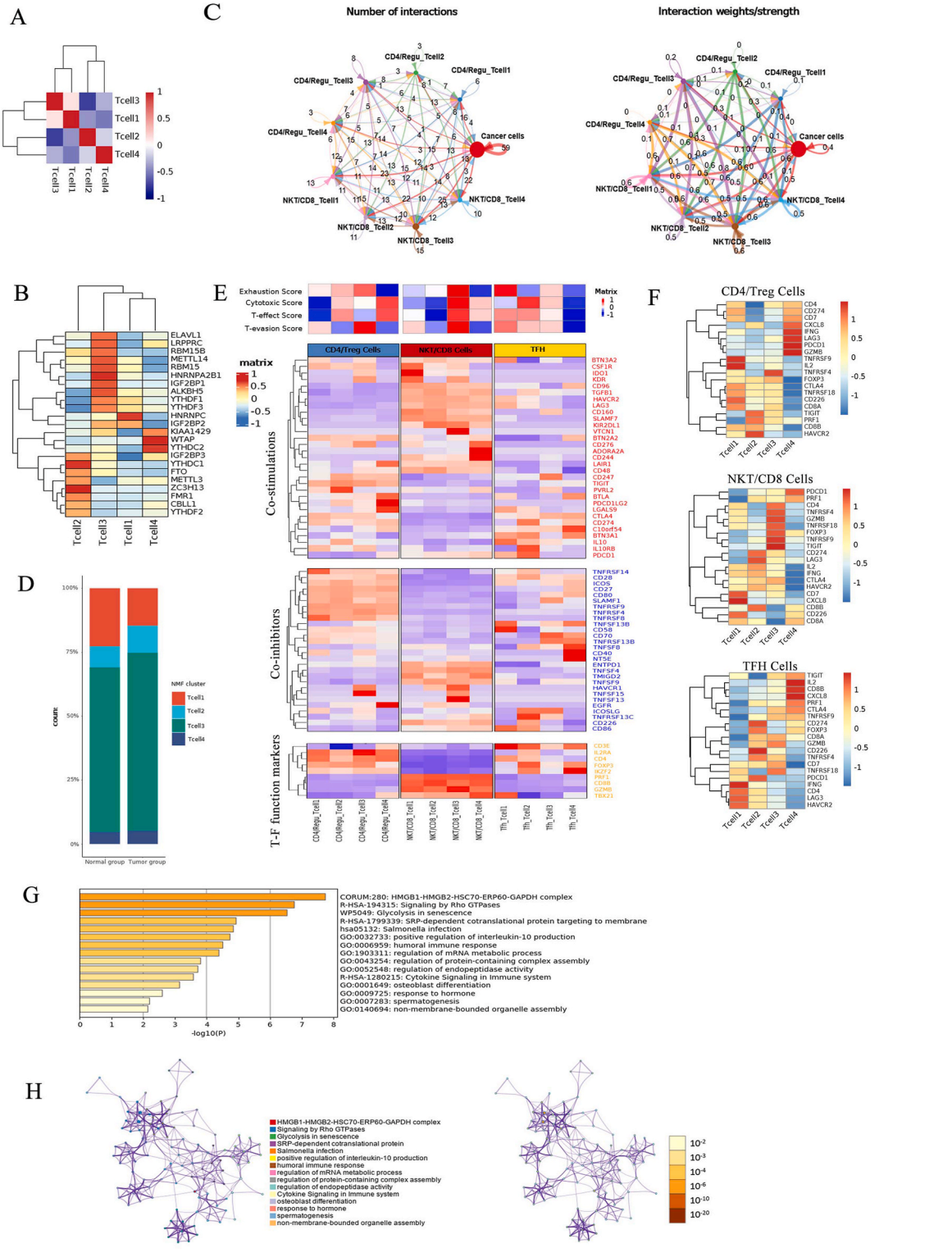

(caption on next page)

Fig. 3. The view of the interaction between the four different m^{6}A-associated T cell clusters. A: The heatmap showed the correlation of the four m^{6}A-associated T cells by NMF; **B**: The heatmap displayed the interactions between the m^{6}A-associated T cell clusters and the cancer cells; **C**: Cell-to-cell interaction network between the m^{6}A-associated T cells and cancer cells; **D**: The bar-plot revealed the different proportion of m^{6}A-associated T cell clusters in the tumor and normal groups. **E**： The heatmap showed the difference between the T scores and the three groups, including CD4$^+$T/Treg cells, CD8$^+$T/NK T cells, and TFH cells by pySCENIC ($p < 0.01$); **F**: The heatmaps revelated the relationship between the m^{6}A-associated T cells clusters and the immune checkpoint associated genes among the three groups; **G**: G.O. and KEGG functional enrichment analysis of the genes in m^{6}A-associated T cell clusters; **H**: Interactions between the enriched pathways across the genes in m^{6}A-associated T cell clusters. The size of the dots denotes the number of genes in the relevant pathway, and the color indicates the cluster type. The paths for the clustering category are given in the tab on the label. Dots representing the same enrichment route have varied colors based on the p-value given on labels. The deeper the dots, the lower the p-value, and the more statistically significant it is. (For interpretation of the references to color in this figure legend, the reader is referred to the Web version of this article.)

dataset contains TME cells from 10 samples from 5 ESCC patients, comprising cancer cells, epithelial cells, endothelial cells, mast cells, myeloid cells, stromal cells, T cells, and B cells (Fig. 1B). Analysis of cell communication revealed relationships between these cell types (Fig. 1C). We compared the expression of m^{6}A regulators in tumor and normal groups (Fig. 1D). The dataset showed differences in the expression levels of m^{6}A regulators in the eight-cell types (Fig. 1E).

3.2. *M^{6}A-mediated macrophages contribute to TME in ESCC patients*

Cell communication analysis showed that m^{6}A-associated macrophages could be divided into four distinct clusters (Fig. 2A), and there were different numbers of ligand-receptor pairs between each cluster and tumor cell cluster (Fig. 2B). We named them as

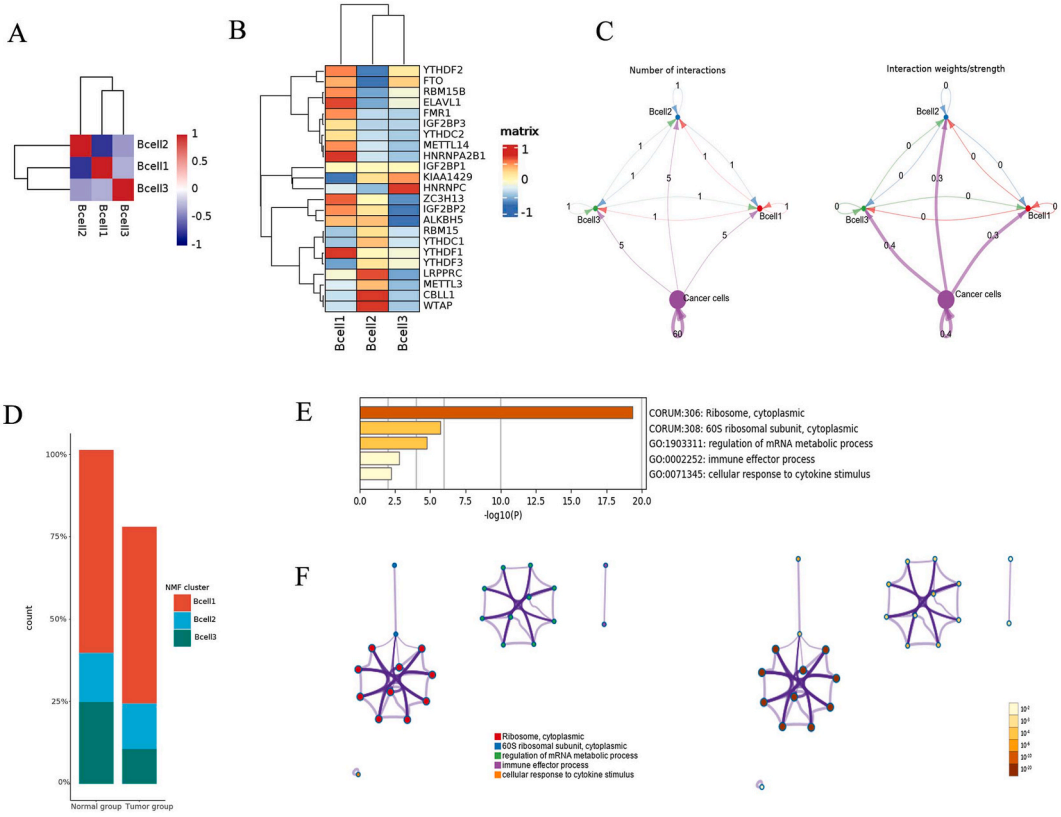

Fig. 4. The view of the interaction between the three different m^{6}A-associated B cell clusters. A: The heatmap showed the correlation of the three m^{6}A-associated B cells by NMF; **B**: The heatmap displayed the interactions between the m^{6}A-associated B cell clusters and the cancer cells; **C**: Cell-to-cell interaction network between the m^{6}A-associated B cells and cancer cells; **D**: The bar-plot revealed the different proportion of m^{6}A-associated B cell clusters in the tumor and normal groups. **E**： G.O. and KEGG functional enrichment analysis of the genes in m^{6}A-associated B cell clusters; **F**: Interactions between the enriched pathways across the genes in m^{6}A-associated T cell clusters. The size of the dots denotes the number of genes in the relevant pathway, and the color indicates the cluster type. The paths for the clustering category are given in the tab on the label. Dots representing the same enrichment route have varied colors based on the p-value given on labels. The deeper the dots, the lower the p-value, and the more statistically significant it is. (For interpretation of the references to color in this figure legend, the reader is referred to the Web version of this article.)

HNRNPC + mac-C1, HNRNPA2B1+mac-C2, WTAP + mac-C3, YTHDC1 & YTHDF2 & YTHDF3 & ZC3H13 +mac-C4 (Fig. 2C). Compared with normal samples, the proportion of YTHDC1 & YTHDF2 & YTHDF3 & ZC3H13 +mac-C4 in tumor samples is higher (Chi-square test $p < 0.001$) (Fig. 2D). Using the AddModulScore function of R-pack Seurat, we found that WTAP + mac-C3 and HNRNPC + mac-C1 were significantly associated with pro-inflammatory macrophages (Fig. 2E). Further, we analyzed the relationship between macrophage clusters and immune checkpoint-associated genes, and the results showed that mac-C3 was strongly connected with CXCL8 and TNFRSF9, mac-C4 was highly associated with CD4 and CD8A, while mac-C2 was significantly correlated with IL2 and CD7, demonstrating that m^{6}A-mediated macrophages are intimately involved with TME (Fig. 2F). GO and KEGG functional enrichment analysis of these m^{6}A-associated macrophages DEGs was conducted to explore their function (Fig. 2G–H, Table S2). Immune cell infiltration and tumor immune microenvironment were shown to be substantially linked with the most significant pathways, including cytokine signaling in the immune system and inflammatory response, which was consistent with the pro-inflammatory effects.

3.3. The m^{6}A-mediated T/B cell subclusters were correlated with the immune response in ERCC

A total of four m6A-associated T-cell clusters were identified by the NMF algorithm (Fig. 3A). These four m6A-associated T cell clusters and the tumor cells each had a distinct number of ligand-receptor pairs (Fig. 3B). Thus we gave them the following names: HNRNPC + T cell-1, YTHDC1&ZC3H13 + T cell-2, HNRNPA2B1+T cell-3 and WTAP + T cell-4, respectively (Fig. 3C). Compared with normal samples, the proportion of HNRNPA2B1+T cell-3 in tumor samples is higher (Fig. 3D). In addition, in order to evaluate the impact that m6A-associated T cell clusters have on T cells, we selected a few co-stimuli that co-inhibit differential expression of immune genes and marker genes that are functionally linked. We also discovered several differences in the average expression of signatures among these m6A clusters of CD4+T/Treg cells, natural killer T cell (NKT)/CD8+T cells, and follicular helper T cell (TFH) cells. There were differences in functional characteristics. Some of these signatures include the T exhaustion score, T cytotoxic score, T effector score, and T evasion score (Fig. 3E). In addition, we also analyzed the relationship between T cells and immune checkpoint genes. The results showed that in CD4+T/Treg cells, T cell-1 was strongly connected with TNFRSF9 and IL2, and T cell-4 was significantly correlated with IFNG, LAG3, and PDCD1. While the correlations showed differences in Tfh cells: T cell-1 was strongly connected with IFNG, T cell-2 was highly associated with CD226, while T cell-4 was significantly correlated with IL2 CD8B and CXCL8. About CD8$^+$ T/NK cells, T cell-1 was strongly connected with CXCL8, and T cell-3 was highly associated with TIGIT (Fig. 3F). GO and KEGG functional enrichment analysis of these m6A-associated T cell DEGs was done to understand their function (Fig. 3G–H, Tables S3–4). NMF analysis revealed that there were three clusters of m6A-associated B cells among the B cells: HNRNPA2B1&YTHDF1&ELAVL1 +B Cell-1, WTAP&CBLL1&LRPPRC + B cell-2, and HNRNPC + B cell-3 (Fig. 4A–C). In tumor groups, HNRNPC + B cell-3 had higher expression (Fig. 4D). GO and KEGG functional enrichment analysis of these m6A-associated B cell DEGs

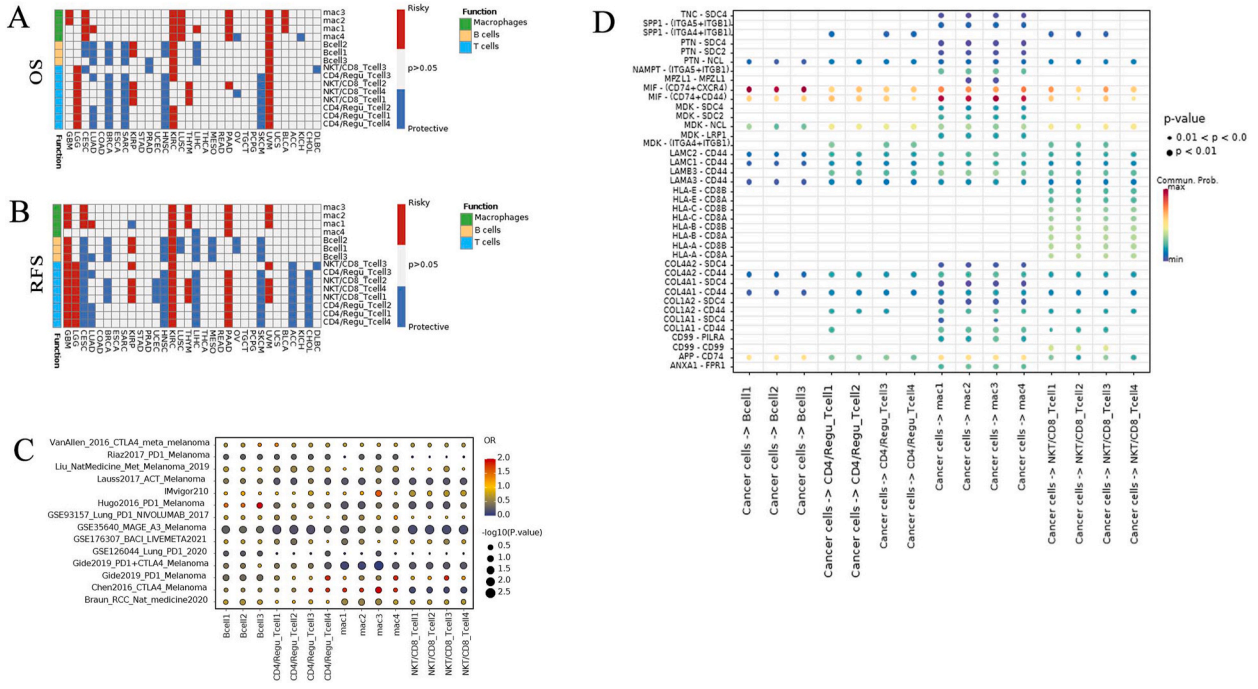

Fig. 5. Overview of the m^{6}A-associated cell clusters and the prognosis as well as the immune therapy. A: The heatmap showed the correlations between m^{6}A-associated cell clusters and the risk level of overall survival (O.S.) in pan-cancers; **B**: The heatmap showed the correlations between m^{6}A-associated cell clusters and the risk level of recurrence-free survival (RFS) in pan-cancers; **C**: Analysis of the relationship between the m^{6}A-associated cell clusters and the immune therapy response; **D**: Analysis of the pair between the m^{6}A-associated cell clusters and cancer cells.

was done to understand their function. The results showed that B cell clusters were related to regulation of mRNA metabolic process and immune effector process (Fig. 4E–F, Table S5).

3.4. The correlation between the m^{6}A-mediated TME and the prognosis and immunotherapy of ESCC

We investigated the correlation between the different m6A-associated cell clusters, including macrophages, T cells, and B cells, with the risk levels of overall survival (OS) or recurrence-free survival (RFS) in pan-cancer. The plot showed that different m^{6}A-associated cell clusters predicting different prognosis in different cancers (Fig. 5A–B). Low-grade glioma (LGG), Kidney renal clear cell carcinoma (KIRC), and Pancreatic adenocarcinoma (PAAD) were closely related to the m6A-associated cell clusters. We used logistic regression analysis to investigate the m^{6}A-associated regulator's clusters and the immune therapy response for patients in 13 public datasets, including melanoma, and urothelial cancer. As the result showed (Fig. 5C), all the cell clusters showed relationships with different immune therapy, which showed promising targets for predicting the effects of immune therapy in different cancers.

3.5. The m^{6}A-mediated cell clusters promoted cell-to-cell communication

Intercellular communication ligand-receptor pairs, including MIF- (CD74+CXCR4) and MIF- (CD74$^+$CD44) ligand-receptor from m^{6}A-associated cell clusters to cancer cells identified by cell-to-cell communication analysis. We found that the m^{6}A-mediated TME cells prompted the communication between the tumor cells and infiltrating immune cells, which were consistent with the different cell subclusters that were responsible for the development of many malignancies that had significant prognoses (Fig. 5D).

3.6. Experimental validation of genes associated with macrophages, T cells, and B cells

The ten patients with ESCC whose genetic testing was completed were provided to us by our hospital. From the normal paracancerous tissues of the patients, the tumor group, we collected tissue RNA. In macrophages, genes YTHDC1, YTHDC2, YTHDC3, and ZC3H13 exhibited higher expression in the tumor group, according to the results of the analysis above. Also, HNRNPA2B1 was expressed higher in the tumor group of T cells, and gene HNRNPC was expressed higher in the tumor group of B cells (Fig. 6).

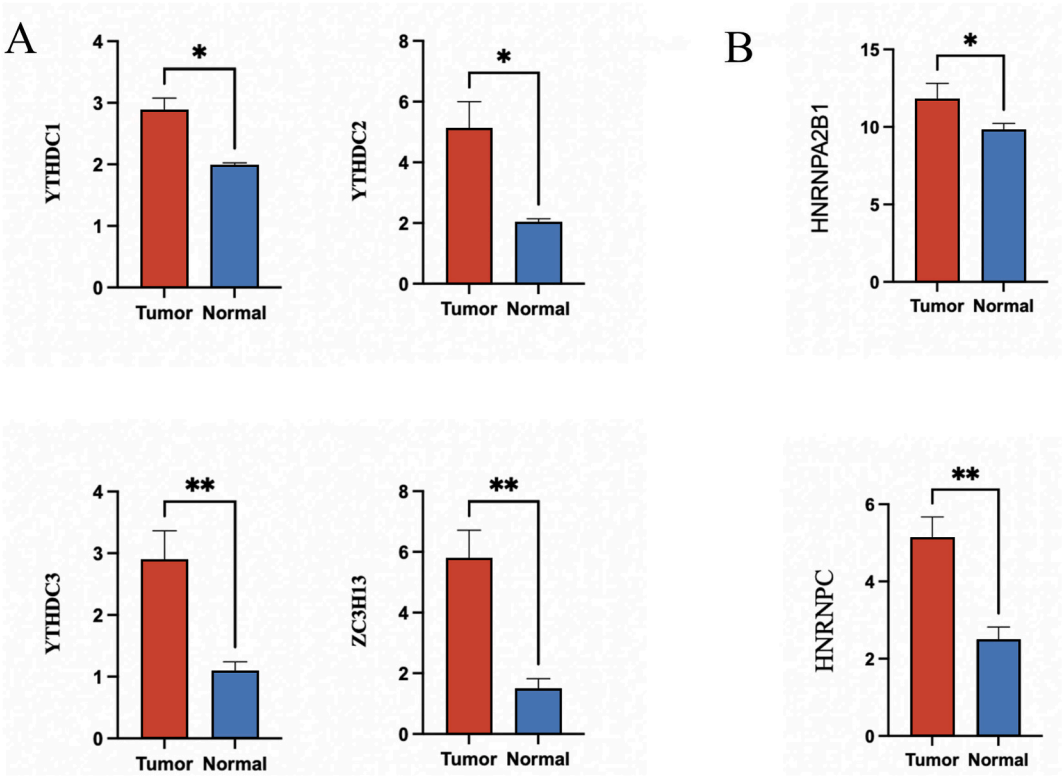

Fig. 6. A Quantitative RT-PCR verifying the expression of YTHDC1, YTHDC2, YTHDC3, and ZC3H13 in macrophages of tumor group and normal paracancerous tissues. *, $p < 0.05$; **, $p < 0.01$; ***, $p < 0.001$; ****, $p < 0.0001$. **B** Quantitative RT-PCR verifying the expression of HNRNPA2B1 in T cells and HNRNPC in B cells of tumor group and normal paracancerous tissues. *, $p < 0.05$; **, $p < 0.01$; ***, $p < 0.001$; ****, $p < 0.0001$.

4. Discussion

Until now, there have been evidence studies explaining the role of RNA m6A methylation modification and the development and development of ESCC [13,14]. However, few studies have demonstrated the role of m^6A-regulated single cells on TME. Our study revealed the main cell clusters of m^6A modification regulators in the TME and explored their expression levels, and their relationship with cancer cells, further investigated the pathway connections between cells and cell clusters and their predictive role in prognosis and immunotherapy response, and comprehensively elucidated the role of m6A RNA methylation and TME in esophageal cancer.

The tumor microenvironment (TME) is an essential factor in carcinogenesis, and immune evasion is a vital step in tumor development, progression, and treatment resistance [47–49]. Macrophages, T cells, and B cells were reported to have a close relationship with ESCC cells. Zhou. et al. [50] reported that M2 macrophages promoted migration and invasion of ESCC. A previous study showed several m6A-associated regulators modulate the immune effects in TME, like ALKBH5 regulating the anti-PD-1 therapy [51]. The interaction among the m6A-associated regulators in TME and the cancer cells in ESCC analyzed by single-cell sequence level showed significant effects. Previous studies showed that m6A may functioned in ESCC through long non-coding RNA (LncRNA) [27,52]. Increasing research has revealed the significance of RNA m^6A methylation in regulating and modulating immune cells [53–56]. A previous study showed that KIF2C expression was significantly tumor-associated macrophages (TAMs), which were involved in m^6A modification [57]. Also , studies have demonstrated that C1q + TAMs are controlled by the m^6A program and regulate tumor-infiltrating $CD8^+$ T cells via the expression of numerous immunomodulatory ligands [55]. Our analysis showed that HNRNPA2B1+mac-C3 was significantly related to SPP1+ and C1q + macrophages and were significantly related to immune pathways. We also found that m^6A-associated T cells, including $CD8^+$, $CD4^+$, and Treg cells, showed close correlation with cancer cells in ESCC, and the main T cells clusters showed different T cell characteristics, which indicated the crucial role of m6A RNA methylation in TME of ESCC.

Our research found that genes YTHDC1, YTHDC2, YTHDC3, and ZC3H13 exhibited higher expression in the tumor group among macrophages, and HNRNPA2B1 was expressed higher in the tumor group of T cells, and gene HNRNPC was expressed higher in the tumor group of B cells. Previous studies showed that YTHDC1 and YTHDC2 [58] were positively related to macrophages [59]. As for other crucial genes, YTHDC2 and ZC3H13 might be associated with the progression of ESCC [60,61], which were corresponded with our results. HNRNPA2B1 was reported to play promoting roles in ESCC progression which was related to p53 mutation [62] and HNRNPC was a key mediator of PD-L1 expression in ESCC [63]. Combining the previous studies and our results, we found that the crucial genes related to m^6A regulator were positively correlated to ESCC.

Considering the complicated intrinsic patterns of RNA m^6A methylation in TME cells, we exhaustively summarized the associations between the scores of various cell clusters and prognosis and response to immunotherapy from the public bulk RNA-seq datasets. Also, ligand-receptor pairs MIF- (CD74+CXCR4) and MIF- ($CD74^+$CD44) revealed the communication between m^6A-associated subtypes of TME cells and cancer cells. Patients with differing levels of m^6A regulators in the TME cells exhibited different ERCC prognostic prediction and immunological responses to ICB treatment, particularly for the macrophages, indicating that TME m^6A played a crucial role in ERCC patients.

This study still has several limitations. First, We only analyzed five ESCC patient samples from our institution. Validation should be performed in larger sample sizes in the GEO database. Besides, the expression levels of the main m6A-associated cell clusters have been validated in qPCR and due to the limitation of the samples from our patients, we faild to validated the results in experiments like Western blot experiments and immunohistochemistry. Also, the interaction between the signaling pathways and cell-to-cell communication deserves more investigation and further explanation. Finally, the English usage of the article needs to be further polished.

Declarations

Ethics approval and participant consent

All participants signed an Informed Consent form by the Helsinki Declaration's ethical criteria. Ethics authorized by the Zhongshan Hospital's ethical committees (B2021 137R).

Author contribution statement

Yunyi Bian: Conceived and designed the experiments; Performed the experiments; Analyzed and interpreted the data; Wrote the paper.

Guoshu Bi: Guangyao Shan: Performed the experiments.

Jiaqi Liang: Qihai Sui: Zhencong Chen: Analyzed and interpreted the data.

Guangyu Yao: Zhengyang Hu: Contributed reagents, materials, analysis tools or data.

Cheng Zhan: Qun Wang: Conceived and designed the experiments.

Data availability statement

Data associated with this study has been deposited at https://www.ncbi.nlm.nih.gov/geo/query/acc.cgi?acc=GSE53625.

Funding statement

This study was funded by the Shanghai Sailing Program (No. 22YF1407500), and the Fellowship of China Postdoctoral Science Foundation (Grant No. 2022M710754).

Declaration of competing interest

The authors declare that they have no known competing financial interests or personal relationships that could have appeared to influence the work reported in this paper.

Appendix A. Supplementary data

Supplementary data to this article can be found online at https://doi.org/10.1016/j.heliyon.2023.e18132.

References

[1] C.C. Abnet, M. Arnold, W.Q. Wei, Epidemiology of esophageal squamous cell carcinoma, Gastroenterology 154 (2018) 360–373.
[2] F. Bray, et al., Global cancer statistics 2018: GLOBOCAN estimates of incidence and mortality worldwide for 36 cancers in 185 countries, CA A Cancer J. Clin. 68 (2018) 394–424.
[3] R. Park, S. Williamson, A. Kasi, A. Saeed, Immune therapeutics in the treatment of advanced gastric and esophageal cancer, Anticancer Res. 38 (2018) 5569–5580.
[4] K. Kato, et al., Nivolumab versus chemotherapy in patients with advanced oesophageal squamous cell carcinoma refractory or intolerant to previous chemotherapy (ATTRACTION-3): a multicentre, randomised, open-label, phase 3 trial, Lancet Oncol. 20 (2019) 1506–1517.
[5] Z.-X. Wang, et al., Toripalimab plus chemotherapy in treatment-naïve, advanced esophageal squamous cell carcinoma (JUPITER-06): a multi-center phase 3 trial, Cancer Cell 40 (2022).
[6] P.C. Tumeh, et al., PD-1 blockade induces responses by inhibiting adaptive immune resistance, Nature 515 (2014) 568–571.
[7] R. Wang, S. Liu, B. Chen, M. Xi, Recent advances in combination of immunotherapy and chemoradiotherapy for locally advanced esophageal squamous cell carcinoma, Cancers 14 (2022).
[8] D. Xiao, et al., m(6)A demethylase ALKBH5 suppression contributes to esophageal squamous cell carcinoma progression, Aging (Albany NY) 13 (2021) 21497–21512.
[9] D. Wu, et al., Long noncoding RNA SNHG12 induces proliferation, migration, epithelial-mesenchymal transition, and stemness of esophageal squamous cell carcinoma cells via post-transcriptional regulation of BMI1 and CTNNB1, Mol. Oncol. 14 (2020) 2332–2351.
[10] M. Li, X. Zha, S. Wang, The role of N6-methyladenosine mRNA in the tumor microenvironment, Biochim. Biophys. Acta Rev. Canc 1875 (2021), 188522.
[11] J.Y. Roignant, M. Soller, m(6)A in mRNA: an ancient mechanism for fine-tuning gene expression, Trends Genet. 33 (2017) 380–390.
[12] L. He, et al., Functions of N6-methyladenosine and its role in cancer, Mol. Cancer 18 (2019) 176.
[13] L. Liao, et al., Anti-HIV drug elvitegravir suppresses cancer metastasis via increased proteasomal degradation of m6A methyltransferase METTL3, Cancer Res. 82 (2022) 2444–2457.
[14] Y. Cui, et al., RNA m6A demethylase FTO-mediated epigenetic up-regulation of LINC00022 promotes tumorigenesis in esophageal squamous cell carcinoma, J. Exp. Clin. Cancer Res. 40 (2021) 294.
[15] E. Azizi, et al., Single-cell map of diverse immune phenotypes in the breast tumor microenvironment, Cell 174 (2018) 1293–1308 e36.
[16] S. Zhou, et al., Roles of highly expressed PAICS in lung adenocarcinoma, Gene 692 (2019) 1–8.
[17] Y.-P. Chen, et al., Single-cell transcriptomics reveals regulators underlying immune cell diversity and immune subtypes associated with prognosis in nasopharyngeal carcinoma, Cell Res. 30 (2020) 1024–1042.
[18] A. Obradovic, et al., Single-cell protein activity analysis identifies recurrence-associated renal tumor macrophages, e16, Cell 184 (2021) 2988–3005.
[19] S. Xing, K. Hu, Y. Wang, Tumor immune microenvironment and immunotherapy in non-small cell lung cancer: update and new challenges, Aging Dis. 13 (2022) 1615–1632.
[20] J. Wei, et al., The roles of plant-derived triptolide on non-small cell lung cancer, Oncol. Res. 27 (2019) 849–858.
[21] Nie Y., et al., NFATc3 promotes pulmonary inflammation and fibrosis by regulating production of CCL2 and CXCL2 in macrophage, Aging Dis. (2023).
[22] L. Wang, H. Cao, Y. Zhong, P. Ji, F. Chen, The role of m6A regulator-mediated methylation modification and tumor microenvironment infiltration in glioblastoma multiforme, Front. Cell Dev. Biol. 10 (2022), 842835.
[23] F.H. Ji, Z. Yang, C. Sun, S. Lowe, X.G. Qiu, Characterization of m6A methylation modifications and tumor microenvironment infiltration in thyroid cancer, Clin. Transl. Oncol. 25 (2023) 269–282.
[24] Z. Chen, et al., Dissecting the single-cell transcriptome network underlying esophagus non-malignant tissues and esophageal squamous cell carcinoma, EBioMedicine 69 (2021), 103459.
[25] S. Zaccara, R.J. Ries, S.R. Jaffrey, Reading, writing and erasing mRNA methylation, Nat. Rev. Mol. Cell Biol. 20 (2019) 608–624.
[26] W. Li, et al., Exosomal FMR1-AS1 facilitates maintaining cancer stem-like cell dynamic equilibrium via TLR7/NFkappaB/c-Myc signaling in female esophageal carcinoma, Mol. Cancer 18 (2019) 22.
[27] Z. Chen, et al., LncRNA FAM83A-AS1 facilitates tumor proliferation and the migration via the HIF-1α/glycolysis axis in lung adenocarcinoma, Int. J. Biol. Sci. 18 (2022) 522–535.
[28] C.S. McGinnis, L.M. Murrow, Z.J. DoubletFinder Gartner, Doublet detection in single-cell RNA sequencing data using artificial nearest neighbors, e4, Cell Syst. 8 (2019) 329–337.
[29] L. Haghverdi, A.T.L. Lun, M.D. Morgan, J.C. Marioni, Batch effects in single-cell RNA-sequencing data are corrected by matching mutual nearest neighbors, Nat. Biotechnol. 36 (2018) 421–427.
[30] Y. Sun, et al., Single-cell landscape of the ecosystem in early-relapse hepatocellular carcinoma, e16, Cell 184 (2021) 404–421.
[31] X. Wu, R. Jiang, M.Q. Zhang, S. Li, Network-based global inference of human disease genes, Mol. Syst. Biol. 4 (2008) 189.
[32] A.P. Patel, et al., Single-cell RNA-seq highlights intratumoral heterogeneity in primary glioblastoma, Science 344 (2014) 1396–1401.
[33] C.B. Steen, C.L. Liu, A.A. Alizadeh, A.M. Newman, Profiling cell type abundance and expression in bulk tissues with CIBERSORTx, Methods Mol. Biol. 2117 (2020) 135–157.
[34] D.A. Barbie, et al., Systematic RNA interference reveals that oncogenic KRAS-driven cancers require TBK1, Nature 462 (2009) 108–112.
[35] F. Ulloa-Montoya, et al., Predictive gene signature in MAGE-A3 antigen-specific cancer immunotherapy, J. Clin. Oncol. 31 (2013) 2388–2395.
[36] W. Hugo, et al., Genomic and transcriptomic features of response to anti-PD-1 therapy in metastatic melanoma, Cell 168 (2017) 542.

[37] D. Liu, et al., Author Correction: integrative molecular and clinical modeling of clinical outcomes to PD1 blockade in patients with metastatic melanoma, Nat. Med. 26 (2020) 1147.
[38] N. Riaz, et al., Tumor and microenvironment evolution during immunotherapy with nivolumab, e16, Cell 171 (2017) 934–949.
[39] S. Mariathasan, et al., TGFbeta attenuates tumour response to PD-L1 blockade by contributing to exclusion of T cells, Nature 554 (2018) 544–548.
[40] D.A. Braun, et al., Interplay of somatic alterations and immune infiltration modulates response to PD-1 blockade in advanced clear cell renal cell carcinoma, Nat. Med. 26 (2020) 909–918.
[41] J.W. Cho, et al., Genome-wide identification of differentially methylated promoters and enhancers associated with response to anti-PD-1 therapy in non-small cell lung cancer, Exp. Mol. Med. 52 (2020) 1550–1563.
[42] E.M. Van Allen, et al., Genomic correlates of response to CTLA-4 blockade in metastatic melanoma, Science 350 (2015) 207–211.
[43] T.N. Gide, et al., Distinct immune cell populations define response to anti-PD-1 monotherapy and anti-PD-1/anti-CTLA-4 combined therapy, Cancer Cell 35 (2019) 238–255 e6.
[44] T. Nathanson, et al., Somatic mutations and neoepitope homology in melanomas treated with CTLA-4 blockade, Canc. Immun. Res. 5 (2017) 84–91.
[45] M. Lauss, et al., Mutational and putative neoantigen load predict clinical benefit of adoptive T cell therapy in melanoma, Nat. Commun. 8 (2017) 1738.
[46] T.L. Rose, et al., Fibroblast growth factor receptor 3 alterations and response to immune checkpoint inhibition in metastatic urothelial cancer: a real world experience, Br. J. Cancer 125 (2021) 1251–1260.
[47] P.M. Aponte, A. Caicedo, Stemness in cancer: stem cells, cancer stem cells, and their microenvironment, Stem Cell. Int. 2017 (2017), 5619472.
[48] T. Lu, et al., Single-cell transcriptome atlas of lung adenocarcinoma featured with ground glass nodules, Cell Discov. 6 (2020) 69.
[49] Z. Chen, et al., Landscape and dynamics of single tumor and immune cells in early and advanced-stage lung adenocarcinoma, Clin. Transl. Med. 11 (2021), e350.
[50] J. Zhou, et al., IL-1beta from M2 macrophages promotes migration and invasion of ESCC cells enhancing epithelial-mesenchymal transition and activating NF-kappaB signaling pathway, J. Cell. Biochem. 119 (2018) 7040–7052.
[51] N. Li, et al., ALKBH5 regulates anti-PD-1 therapy response by modulating lactate and suppressive immune cell accumulation in tumor microenvironment, Proc. Natl. Acad. Sci. U. S. A. 117 (2020) 20159–20170.
[52] Y. Cui, et al., RNA m6A demethylase FTO-mediated epigenetic up-regulation of LINC00022 promotes tumorigenesis in esophageal squamous cell carcinoma, J. Exp. Clin. Cancer Res. : CR 40 (2021) 294.
[53] H. Yin, et al., RNA m6A methylation orchestrates cancer growth and metastasis via macrophage reprogramming, Nat. Commun. 12 (2021) 1394.
[54] D. Han, et al., Anti-tumour immunity controlled through mRNA m6A methylation and YTHDF1 in dendritic cells, Nature 566 (2019) 270–274.
[55] L. Dong, et al., The loss of RNA N(6)-adenosine methyltransferase Mettl14 in tumor-associated macrophages promotes CD8(+) T cell dysfunction and tumor growth, e10, Cancer Cell 39 (2021) 945–957.
[56] J. Tong, et al., m(6)A mRNA methylation sustains Treg suppressive functions, Cell Res. 28 (2018) 253–256.
[57] X. Zhang, Y. Li, P. Hu, L. Xu, H. Qiu, KIF2C is a biomarker correlated with prognosis and immunosuppressive microenvironment in human tumors, Front. Genet. 13 (2022), 891408.
[58] F. Yin, et al., The effect of N6-methyladenosine regulators and m6A reader YTHDC1-mediated N6-methyladenosine modification is involved in oxidative stress in human aortic dissection, Oxid. Med. Cell. Longev. 2023 (2023), 3918393.
[59] X. Ge, et al., The loss of YTHDC1 in gut macrophages exacerbates inflammatory bowel disease, Adv. Sci. 10 (2023), e2205620.
[60] N. Yang, et al., Genetic variants in m6A modification genes are associated with esophageal squamous-cell carcinoma in the Chinese population, Carcinogenesis 41 (2020) 761–768.
[61] H.-S. Yang, et al., A novel ras–related signature improves prognostic capacity in oesophageal squamous cell carcinoma, Front. Genet. 13 (2022), 822966.
[62] R. Feng, et al., Mutant p53 activates hnRNPA2B1-AGAP1-mediated exosome formation to promote esophageal squamous cell carcinoma progression, Cancer Lett. 562 (2023), 216154.
[63] W. Guo, et al., Comprehensive analysis of PD-L1 expression, immune infiltrates, and m6A RNA methylation regulators in esophageal squamous cell carcinoma, Front. Immunol. 12 (2021), 669750.